Air flow in sanitary sewer conduits due to wastewater drag: a computational fluid dynamics approach[1]

S. Edwini-Bonsu and P.M. Steffler

Abstract: An accurate calculation of air flow in sanitary sewer conduits is a key input for improved understanding of odorous-compound emissions, efficient design of ventilation systems, and the occurrence of sewer fabric corrosion. In this study, the driving force of wastewater drag is considered and conceptually viewed as a Couette flow. Both turbulent and laminar flow regimes are modeled. In the turbulent flow regime, the Reynolds-averaged-Navier-Stokes equations are closed with an anisotropic turbulence model that consists of two sub-models: a generalized eddy viscosity mixing length model for the turbulent shear stresses and a semi-empirical model for the turbulent normal stresses. Solution of the resulting set of parabolic equations is implemented in a Gelerkin finite element framework. The predictive performances of the models are in agreement with longitudinal velocity measurements reported in the literature. Although the secondary flows computed are within a few percentage of the main flow velocity, the mean flow field is affected considerably by the secondary currents in every case. The present study suggests that models currently in use for estimating ventilation rates in sewer drains generally over predict the turbulent streamwise mean velocity.

Key words: air flow, computational fluid dynamics, finite element method, mixing length, sewer conduit, turbulence-driven secondary currents, ventilation model, wastewater drag.

Résumé : Un calcul précis de l'écoulement d'air dans les conduits sanitaires est un intrant clé pour mieux comprendre les émissions de composés odorants, la conception efficace des systèmes de ventilation et l'apparition de corrosion de la structure des égouts. Dans cette étude, la force à la base de la résistance à l'écoulement des eaux usées est considérée comme étant un écoulement de Couette et considérée théoriquement ainsi. Les régimes d'écoulement turbulent et laminaire sont modélisés. Dans le régime turbulent, les équations de type RANS (Reynolds-averaged Navier-Stokes) sont complétées par un modèle de turbulence anisotrope qui comporte deux sous-modèles : un modèle généralisé de longueur de mélange à viscosité tourbillonnaire pour les tensions de Reynolds et un modèle semi-empirique pour les tensions normales turbulentes. La solution de l'ensemble d'équations paraboliques obtenues est implantée dans la méthode de Gelerkin aux éléments finis. Les rendements prédictifs des modèles sont conformes aux mesures des vitesses longitudinales rapportées dans la littérature. Bien que les débits secondaires calculés soient à l'intérieur d'une plage de quelques points de pourcentage de la vitesse du débit principal, le champ de courant moyen est considérablement touché par les courants secondaires dans chaque cas. La présente étude suggère que les modèles actuellement utilisés pour estimer les taux de renouvellement d'air dans les conduites d'égout prédisent des valeurs de vélocité moyenne turbulente dans la direction d'écoulement généralement supérieures aux observations.

Mots clés : écoulement d'air, dynamique des fluides numérique, méthode des éléments finis, longueur de mélange, conduite d'égout, courants secondaires causés par les remous, modèle de ventilation, résistance à l'écoulement des eaux usées.

[Traduit par la Rédaction]

Introduction

Air flow modeling in sanitary sewer conduits is a key input for efficient design of ventilation systems and for improved understanding of emission of volatile organic compounds (VOCs) from and occurrence of corrosion in sewer piping systems (Bowker et al. 1989; Matos and de Sousa 1992; Pescod and Price 1978; Odor and Corrosion Technology Consultants 1999*b*; Olson et al. 1997; Quigley and Corsi 1995). Unfortunately, collection systems are designed to only carry liquid flow without regard to what happens to the airspace. Therefore the effects of friction drag, acceleration and deceleration of wastewater,

Received 26 June 2003. Revision accepted 8 October 2003. Published on the NRC Research Press Web site at http://jees.nrc.ca/ on 24 September 2004.

S. Edwini-Bonsu[2] and P.M. Steffler. Department of Civil and Environmental Engineering, 220 Civil/Elect. Building, University of Alberta, Edmonton, AB T6G 2G7, Canada.

Written discussion of this article is welcomed and will be received by the Editor until 31 January 2005.

[1]This article is one of a selection of papers published in this Special Issue on Environmental Hydraulics.

[2]Corresponding author (e-mail: edwinibo@ualberta.ca).

 doi: 10.1139/S03-072

and headspace pressurization are largely misunderstood and ignored. As a consequence, the movement of air into, along, and out of wastewater collection systems is for the most part uncontrolled. This causes odour complaints and points of aggressive corrosion that may be totally unexpected and are identified only after system startup.

Field and laboratory studies indicate that wastewater drag and other natural factors such as differential wind speed and barometric pressure gradient are the major forces responsible for air flow in sanitary sewer channels (Pescod and Price 1978, 1981, 1982; Pomeroy 1945; Odor and Corrosion Technology Consultants 1999*b*; Olson 1996; Olson et al. 1997; Quigley and Corsi 1995; USEPA 1994; Thistlethwayte 1972). The effects of these driving forces do not only accelerate the sewer air along the sewer pipe, but also cause air ejection and hence odour releases via available openings. Air movement resulting from barometric pressure and wind speed has been studied using computational fluid dynamics (CFD) techniques by Edwini-Bonsu and Steffler (2003) and also studied somewhat quantitatively or qualitatively in the literature (Pescod and Price 1978, 1981, 1982; Olson 1996; Olson et al. 1997; USEPA 1994).

In this study, only the driving force of wastewater drag is considered. Wastewater flowing down the sewer results in friction at the air–water interface and this translates into an induced flow of air. Of all the factors that affect the movement of sewer gases, the wastewater drag is the one that acts continuously. With no other ventilation mechanism present, air and wastewater flow should be co-current. However, recirculation flow patterns may exist when openings between sewer and ambient atmospheres are restricted (Olson 1996). Quigley and Corsi (1995) measured air exchange rates using both anemometric method and sulphur hexafluoride injections within a municipal sewer interceptor. The system conveyed wastewater containing significant industrial discharges and was characterized by numerous openings for air exchange. Air exhaust rates from a single manhole cover containing 66 1-inch (1 in. = 2.54 cm) diameter pickholes ranged from a low of 140 m^3/h at 6 a.m. to a high of 590 m^3/h at 12 p.m. The profile of air exchange rates was consistent with wastewater flow rates, suggesting that ventilation was driven by liquid drag. Pescod and Price (1978) also referenced field studies in Tyneside sewerage scheme in England. The sewer section studied had an internal diameter of 1650 mm and slope of 1/202. During the time of the tests, sewage was flowing at a depth of 150–200 mm and a surface velocity of about 1 m/s. The measured air flow rates within the sewer ranged from 105 to 315 m^3/h.

Pescod and Price (1978) were perhaps the first to present scientific experimental studies on wastewater-driven air movement in sewer atmosphere. They conducted laboratory anemometric air velocity measurements and developed empirical curves for the estimation of the average air velocity. Nonetheless their curves did not adequately characterize the complete interactions of this motive force and possible range of sewer hydraulic conditions. In a related field study Pescod and Price (1978) indicated that their empirical models are not directly applicable to sewer diameters larger than the one used in their laboratory studies and that predictions could be higher. In response to the limited knowledge base associated with hazardous air pollutant (HAP) emissions from industrial sewers, the United States Environmental Protection Agency (USEPA) commissioned the development of a model that estimates emissions from sewers (USEPA 1994). This model is expected to predict higher rates since no consideration is given to the possibility of interfacial waves and upshots of secondary motions associated with the shape of the headspace. Interestingly this model is the only one currently available for estimating ventilation rates from drains due to wastewater regardless of the flow regime. Olson (1996) and Olson et al. (1997) theoretically studied the effects of liquid drag in industrial sewer drains using energy concepts. They identified two forces acting on the air as the liquid drag (at the air–water interface) and the shear stress at the pipe wall. These two forces were then quantified using empirical modeling and boundary layer theory. The major problems of their approach are the use of an oceanic-resistance model (a modified Charnock-Sinai based model (Sinai 1983)) at the air–water interface, which is completely different in character from internal gravity flow, and the treatment of the headspace as a 1-D channel. A very crude approach, presumably based on the premise of a 1-D flow field, is also in use (Odor and Corrosion Technology Consultants 1999*a*). This method simply assumes that the average air velocity is one half the average wastewater velocity irrespective of the sewer hydraulics.

Clearly, there are inadequacies in the existing models. Any improvement in the flow modeling, therefore, should include more physics, and correct representation of the airspace cross section and the driving force. Furthermore, the improvement should not be limited to the mean streamwise average velocity computations, but also offer a thorough understanding of the flow patterns in the sewer headspace. This is especially relevant in corrosion modeling. The present paper therefore introduces CFD models for predicting the air flow field in which the Reynolds-averaged-Navier-Stokes (RANS) equations with incompressible, fully developed, and steady-state assumptions govern the flow field. The Reynolds stresses in the governing equations are computed using an anisotropic turbulence model that takes into account the effect of the sewer headspace geometry to generate turbulence-driven secondary flows. This consists of two sub-models: a generalized eddy viscosity mixing length model for the shear stresses and a semi-empirical model for the normal stresses. A finite element solution of the resulting set of parabolic equations is implemented. The effect of wastewater drag is formulated at the air–wastewater interface as in single flows. To cover all possible flow scenarios, a laminar model is also developed. Calculations from these models are compared with experimental data from Pescod and Price (1978) and the above-mentioned ventilating models. Generalized curves and formulae for the mean velocities have been developed to be used in practice since it would be too difficult to use the full CFD models.

Mathematical formulation

Mean flow equations

Figure 1 shows a schematic representation of a partially full, gravity-flow circular sewer conduit, including the coordinate system and nomenclature. We assume an isolated section of the wastewater collection system without intersecting sewer lines, changes in channel slope, or changes in pipe diameter thus making the assumption of fully-developed flow ($\partial(..)/\partial x = 0$) strictly valid. Steady (time-invariant, $\partial(..)/\partial t = 0$) state condition is further assumed. Under the aforementioned assumptions, the Reynolds-averaged-Navier-Stokes equations together with the continuity equation of turbulent incompressible flow lead to

$$[1a] \quad V\frac{\partial U}{\partial y} + W\frac{\partial U}{\partial z} = g\sin\beta + \nu\left(\frac{\partial^2 U}{\partial y^2} + \frac{\partial^2 U}{\partial z^2}\right) - \left(\frac{\partial \overline{u'v'}}{\partial y} + \frac{\partial \overline{u'w'}}{\partial z}\right)$$

$$[1b] \quad V\frac{\partial V}{\partial y} + W\frac{\partial V}{\partial z} = -\frac{1}{\rho}\frac{\partial P}{\partial y} + g\cos\beta + \nu\left(\frac{\partial^2 V}{\partial y^2} + \frac{\partial^2 V}{\partial z^2}\right) - \left(\frac{\partial \overline{v'^2}}{\partial y} + \frac{\partial \overline{w'v'}}{\partial z}\right)$$

$$[1c] \quad V\frac{\partial W}{\partial y} + W\frac{\partial W}{\partial z} = -\frac{1}{\rho}\frac{\partial P}{\partial z} + \nu\left(\frac{\partial^2 W}{\partial y^2} + \frac{\partial^2 W}{\partial z^2}\right) - \left(\frac{\partial \overline{v'w'}}{\partial y} + \frac{\partial \overline{w'^2}}{\partial z}\right)$$

$$[1d] \quad \frac{\partial V}{\partial y} + \frac{\partial W}{\partial z} = 0$$

where P is the total pressure, i.e., the sum of pressure resulting from the normal components of the molecular forces and the pressure arising from anisotropy of turbulence, υ and ρ are, respectively, the kinematic viscosity and density of air, U is the streamwise mean velocity in the x direction, g is the acceleration due to gravity, β is the slope of the sewer pipe. u', v', and w' are components of the turbulent velocities in the x, y, and z directions, respectively. The velocities V and W are secondary mean flow in the plane perpendicular to the primary longitudinal (x) direction. These secondary velocities are caused by the anisotropy of the normal Reynolds stress terms $\overline{v'^2}$ and $\overline{w'^2}$ (Demuren and Rodi 1984; Gerard 1978; Rodi 1984).

The Reynolds stresses in the mean flow equations have to be modeled. The simplest turbulence models employ the Boussinesq eddy viscosity approximation to compute the Reynolds stresses. For computational simplicity, the eddy viscosity is, in turn, often computed in terms of the mixing length that is analogous to the mean free path of molecules in the kinetic theory of gases. Prandtl's mixing length hypothesis (MLH) is among the simplest turbulence models for modeling the turbulent shear

Fig. 1. Idealized sewer conduit model.

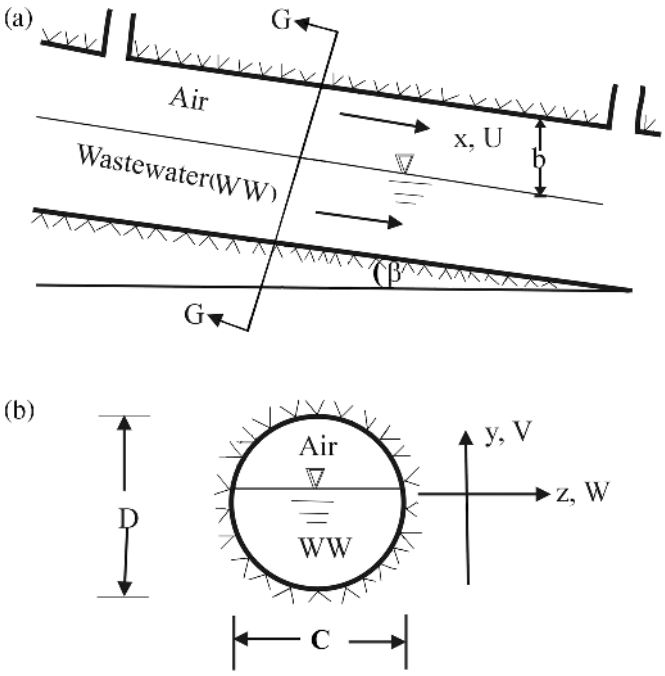

stresses. Unfortunately, Prandtl's MLH does not include any information on the normal stresses. For homogenous turbulence, the normal stresses are usually included in the pressure and they do not have to be calculated. This is not the case here, because the flow in the headspace is not homogeneous. Thus, in addition to specifying the shear stresses, modeling of the turbulent normal stresses is needed. This problem is discussed below.

Turbulence closure

The Reynolds stresses appearing in eqs. [1*a*]–[1*c*] are modeled via an anisotropic turbulence closure model that comprises the use of an eddy viscosity concept for the shear stresses and a semi-empirical model for the normal stresses. This approach allows us to compute the turbulence-driven secondary motions owing to the differences in the normal stresses ($\overline{v'^2} - \overline{w'^2}$).

Modeling the Reynolds shear stresses

The eddy viscosity concept that is based on the assumption that the Reynolds stresses are a local property of the mean flow and are related to the mean flow gradients via a turbulent viscosity is used. For the flow under consideration this concept may be expressed as

$$[2a] \quad -\overline{u'v'} = \nu_t\frac{\partial U}{\partial y}$$

$$[2b] \quad -\overline{u'w'} = \nu_t\frac{\partial U}{\partial z}$$

$$[2c] \quad -\overline{v'w'} = \nu_t\left(\frac{\partial W}{\partial y} + \frac{\partial V}{\partial z}\right)$$

where ν_t is the eddy viscosity. The introduction of eq. [2] alone does not constitute a turbulent model for the shear stresses, but only offers the framework for constructing such a model; the main problem is now shifted to determining the distribution of ν_t. There are several ways of determining this distribution (Rodi 1984). In a preliminary study two closure models have been investigated. These are the low Reynolds number k–ε model of Lam and Bremhorst (1981), and a generalized bi-harmonic mixing length model of Robert et al. (1998). Although these models give comparable average longitudinal mean velocities, the mixing length model provides better air velocity patterns in the headspace (in comparison with experimental data from Pescod and Price 1978). In view of this, the mixing length model has been chosen for this study.

Hence the eddy viscosity is obtained from a generalized mixing length formulation given as (Rodi 1984)

$$[3] \qquad \nu_t = l_m^2 \left[\left(\frac{\partial U_i}{\partial X_j} + \frac{\partial U_j}{\partial X_i} \right) \frac{\partial U_i}{\partial X_j} \right]^{1/2}$$

wherein the Einstein's summation is used. The l_m term is the mixing length. Equation [3] in a fully-developed 3-D flow is expanded as

$$[4] \qquad \nu_t = l_m^2 \left[\left(\frac{\partial U}{\partial y} \right)^2 + \left(\frac{\partial U}{\partial z} \right)^2 + 2 \left(\frac{\partial V}{\partial y} \right)^2 + 2 \left(\frac{\partial W}{\partial z} \right)^2 + \left(\frac{\partial V}{\partial z} + \frac{\partial W}{\partial y} \right)^2 \right]^{1/2}$$

The mixing length is prescribed using the Robert et al. (1998) bi-harmonic model, which is given as

$$[5] \qquad \frac{\partial^4 l_m}{\partial z^4} + 2 \frac{\partial^4 l_m}{\partial z^2 \partial y^2} + \frac{\partial^4 l_m}{\partial y^4} = 0$$

with the rigid boundary conditions

$$[6a] \qquad l_m = 0$$

$$[6b] \qquad \frac{\partial l_m}{\partial n} = -\kappa$$

where n is the normal outside the domain on the boundaries and κ is the von Karman's constant. These formulations make the mixing length concept applicable to complex geometries thus removing the bottlenecks associated with Prandtl's original mixing length hypothesis.

Modeling the Reynolds normal stresses

To calculate the secondary velocities, the distribution of the main driving forces (Reynolds normal stresses) needs to be determined. To obtain a visual impression of the circulation due to secondary flows, Gerard (1978) pioneered a semi-empirical approach that enabled the prediction of the secondary flow streamlines. Tominaga et al. (1989) have successfully modified Gerard's approach and verified it experimentally. Tominaga et al. (1989) derived a semi-empirical relation for the distribution of $\sqrt{\overline{v'^2}}$ and $\sqrt{\overline{w'^2}}$ for a two-dimensional closed-channel as

$$[7] \qquad \begin{aligned} \sqrt{\overline{v'^2}}(y) &= u_\tau \left[A_{vy} \exp\left(-B_{vy} \frac{y}{h} \right) \right] \\ \sqrt{\overline{w'^2}}(y) &= u_\tau \left[A_{wy} \exp\left(-B_{wy} \frac{y}{h} \right) \right] \end{aligned}$$

where $A_{wy} = 1.45$, $A_{vy} = 1.15$, $B_{wy} = 0.92$, $B_{vy} = 0.69$, h is the depth of the channel, and u_τ is the boundary shear velocity. Using a weighted average method, Tominaga et al. (1989) extended these semi-empirical formulations to three-dimensions. Czernuszenko and Rylov (2002) have successfully employed a version of Tominaga et al.'s relations for open channels in modeling a three-dimensional velocity field in open-channel flows. The pattern of secondary flow was accurately simulated. Here semi-empirical relations of Tominaga et al. (1989) are adopted for the normal stresses given in this case as

$$[8a] \qquad \begin{aligned} \sqrt{\overline{v'^2}}(n_i) &= u_{\tau i} \left[A_{vn} \exp\left(-B_{vn} n_i \right) \right] \\ \sqrt{\overline{v'^2}}(n_w) &= u_{\tau w} \left[A_{vn} \exp\left(-B_{vn} n_w \right) \right] \end{aligned}$$

$$[8b] \qquad \begin{aligned} \sqrt{\overline{w'^2}}(n_i) &= u_{\tau i} \left[A_{wn} \exp\left(-B_{wn} n_i \right) \right] \\ \sqrt{\overline{w'^2}}(n_w) &= u_{\tau w} \left[A_{wn} \exp\left(-B_{wn} n_w \right) \right] \end{aligned}$$

where $A_{wn} = 1.45$, $A_{vn} = 1.15$, $B_{wn} = 0.92$, $B_{vn} = 0.69$. The weighted average contribution from the wall and the interface is expressed as

$$[9] \qquad \begin{aligned} \sqrt{\overline{v'^2}} &= \left(\sqrt{\overline{v'^2}}(n_i) \right)^{\Gamma_{n_i}} \left(\sqrt{\overline{v'^2}}(n_w) \right)^{\Gamma_{n_w}} \\ \sqrt{\overline{w'^2}} &= \left(\sqrt{\overline{w'^2}}(n_i) \right)^{\Gamma_{n_i}} \left(\sqrt{\overline{w'^2}}(n_w) \right)^{\Gamma_{n_w}} \end{aligned}$$

where $\Gamma_{n_i} = n_w/(n_w + n_i)$, $\Gamma_{n_w} = n_i/(n_w + n_i)$, n_i and n_w are dimensionless normal distances from the interface and the wall, respectively.

Computational approach

The air flow in the sewer atmosphere could be laminar, turbulent, or transitional contingent upon the magnitude of the driving force. Pescod and Price (1978) and Olson (1996) reported low Reynolds number flow regimes in their studies. It has been reported that the friction between the wastewater and air can be increased through steep slopes or wastewater velocities in excess of 1.5 m/s (Odor and Corrosion Technology Consultants 1999*b*). Given this added impact of increased friction, the volume of moving air can be quite large and turbulent. Consequently any modeling technique should take these regimes into consideration. Here, the transitional regime is not considered. Discussed below are the boundary conditions and the numerical solution methods for the two regimes of interest.

Boundary conditions

Boundary conditions are required at the wall and the interface. In the present study the integration of the flow equations is carried out to the wall, which makes the no-slip condition applicable. This means that the velocities tangential and normal to the wall are zero. The use of the no-slip condition calls for a modification of the mixing length boundary condition (eq. [6*b*]). This is realized by applying the Van Driest damping function (Wilcox 2000) to bridge the fully turbulent zones away from the wall and the near-wall regions where viscosity effects are substantial such that

$$[10] \qquad \frac{\partial l_{\mathrm{m}}}{\partial n} = -\kappa\left[1-(1+S(n))\exp(S(n))\right]$$

where $S(n) = -nu_\tau/vA$ and A is an empirical constant equal to 26.

Throughout this paper, it is assumed that there is negligible momentum transfer from the air to the underlying wastewater. This assumption is adequate since the air motion is caused by the air being dragged along by the wastewater (i.e., without the wastewater there is no air flow). The air–water interface is hence modeled as a rigid-moving lid as in Couette flows. Practically, the interface may not be sharp and could contain a mixture of air and water with concomitant generation of waves and "whitecaps" (Odor and Corrosion Technology Consultants 1999*b*). Consequently the interface should be treated with caution if detailed features are required. Four possible cases for prescribing the interfacial boundary for the mean longitudinal velocity are proposed.

- Smooth interface

$$[11] \qquad U = U_{\mathrm{w}}$$

- Rippled interface (small amplitude and well-organized waves)

$$[12] \qquad U = U_{\mathrm{ws}}$$

- Rippled interface (large amplitude and well-organized waves)

$$[13] \qquad \frac{U-U_{\mathrm{ws}}}{u_{\tau\mathrm{i}}} = -\frac{1}{\kappa}\ln(9y^+)$$

- Fully rough interface (a precursor to a transition to slug flow)

$$[14] \qquad \frac{U-U_{\mathrm{ws}}}{u_{\tau\mathrm{i}}} = -\frac{1}{\kappa}\ln\left(\frac{9y^+}{1+0.3k_{\mathrm{s}}^+}\right)$$

where U_{w} is the average water surface velocity, U_{wc} is the water surface velocity at center of pipe, U_{ws} is the surface velocity distribution (eq. [15]), $k^+ = u_{\tau\mathrm{i}}k_{\mathrm{s}}/v$, $y^+ = u_{\tau\mathrm{i}}n_{\mathrm{i}}/v$, and k_{s} is the effective interfacial boundary roughness height. The application of the fully rough interface regime requires knowledge of the interfacial boundary roughness parameter, k_{s}. This regime is likely to occur in very steep slopes. Following Nordsveen and Bertelsen (1996), a relation between the water surface velocity at channel center U_{wc} and velocity distribution at the interface U_{ws} is obtained as

$$[15] \qquad U_{\mathrm{ws}}(z) = U_{\mathrm{wc}}\left(\frac{C-2|z|}{C}\right)^{1/4}$$

where C is the width of the interface. In modeling the laminar flow, it is assumed that the air–water interface is devoid of interfacial waves and therefore the assumptions of smooth interfacial boundary and constant interfacial drag are satisfactory. In this paper eq. [12] together with eq. [15] is used as a boundary condition for all simulated turbulent flows. This boundary condition is justified since we are dealing with large diameter pipes (Vlachos et al. 1999). Secondary velocities are assigned zero at the interface.

Numerical solution

For computational reasons, all variables are nondimensionalized as $X_* = x/b$, $Y_* = y/b$, $Z_* = z/b$, $U_* = U/U_{\mathrm{wc}}$, $V_* = V/U_{\mathrm{wc}}$, $W_* = W/U_{\mathrm{wc}}$, $\overline{v_*'^2} = \overline{v'^2}/U_{\mathrm{wc}}^2$, $\overline{w_*'^2} = \overline{w'^2}/U_{\mathrm{wc}}^2$, and $g_* = gb/U_{\mathrm{wc}}^2$, where the length scale b is the maximum headspace depth and U_{wc} is the velocity scaling parameter in turbulent flow case. The Reynolds number then becomes $Re_{\mathrm{c}} = U_{\mathrm{wc}}b/v$ in the turbulent flow case. Using the turbulent closure models introduced above, the system of equations to solve, in dimensionless forms, becomes

$$[16a] \quad V_*\frac{\partial U_*}{\partial Y_*} + W_*\frac{\partial U_*}{\partial Z_*} - \frac{\partial}{\partial Y_*}\left[(1/Re_{\mathrm{c}}+\nu_{t*})\frac{\partial U_*}{\partial Y_*}\right] - \frac{\partial}{\partial Z_*}\left[(1/Re_{\mathrm{c}}+\nu_{t*})\frac{\partial U_*}{\partial Z_*}\right] = g_*\sin\beta$$

$$[16b] \quad V_*\frac{\partial V_*}{\partial Y_*} + W_*\frac{\partial V_*}{\partial Z_*} - \frac{1}{Re_{\mathrm{c}}}\left[\frac{\partial^2 V_*}{\partial Y_*^2}+\frac{\partial^2 V_*}{\partial Z_*^2}\right] = g_*\cos\beta - \frac{\partial P_*}{\partial Y_*} - \frac{\partial \overline{v_*'^2}}{\partial Y_*} + \frac{\partial}{\partial Z_*}\left[\nu_{t*}\left(\frac{\partial V_*}{\partial Z_*}+\frac{\partial W_*}{\partial Y_*}\right)\right]$$

$$[16c] \quad V_*\frac{\partial W_*}{\partial Y_*} + W_*\frac{\partial W_*}{\partial Z_*} - \frac{1}{Re_{\mathrm{c}}}\left[\frac{\partial^2 W_*}{\partial Y_*^2}+\frac{\partial^2 W_*}{\partial Z_*^2}\right] = -\frac{\partial P_*}{\partial Z_*} - \frac{\partial \overline{w_*'^2}}{\partial Z_*} + \frac{\partial}{\partial Y_*}\left[\nu_{t*}\left(\frac{\partial V_*}{\partial Z_*}+\frac{\partial W_*}{\partial Y_*}\right)\right]$$

$$[16d] \quad \frac{\partial V_*}{\partial Y_*} + \frac{\partial W_*}{\partial Z_*} = 0$$

$$[17]\quad \nu_{t*} = l_{m*}^2 \left[\left(\frac{\partial U_*}{\partial Y_*}\right)^2 + \left(\frac{\partial U_*}{\partial Z_*}\right)^2 + 2\left(\frac{\partial V_*}{\partial Y_*}\right)^2 + 2\left(\frac{\partial W_*}{\partial Z_*}\right)^2 + \left(\frac{\partial V_*}{\partial Z_*} + \frac{\partial W_*}{\partial Y_*}\right)^2 \right]^{1/2}$$

In laminar flow, the flow field has only one component $U_*(Y_*, Z_*)$ and the remaining governing equation simply reduces to

$$[18]\quad -\frac{\partial}{\partial Y_*}\left[(1/Re_w)\frac{\partial U_*}{\partial Y_*}\right] - \frac{\partial}{\partial Z_*}\left[(1/Re_w)\frac{\partial U_*}{\partial Z_*}\right] = g_* \sin\beta$$

Here, U_w is used as the velocity scaling parameter and the Reynolds number of the flow becomes $Re_w = U_w b/v$. The upper limit of the laminar flow regime is set at a Reynolds number of 1500 based on a plane Couette flow of moving wall velocity U_w and depth of flow b (Wilcox 2000).

In preliminary test computations, the laminar formulation (eq. [18]) has been solved using analytical, finite difference, and finite element methods. The first two methods have been used with the primary aim of checking the predictive capability of the finite element discretization scheme, which is the core numerical tool in this paper. In the analytical method, the airspace cross section is approximately transformed into half-elliptic shape facilitating the use of elliptic orthogonal and conformal curvilinear coordinates. The resulting equation is subsequently solved using the method of eigenfunction expansion. The finite difference approach uses the generalized coordinates system and employs the transfinite algebraic grid generation technique to transform the governing equation and the flow geometry into a body-fitted unit-square coordinates system that allows coincidence of all boundary lines with a coordinate line. The discretization is then evaluated using central difference formulae. Satisfactory agreements have been obtained between the finite element scheme and the other two methods. The preference of the finite element method to the other computational techniques stems from its capability to handle complex flow geometries, consistency, and generality.

The finite element method (FEM) implemented here is based on the FEMLAB programming language that stores data structures in MATLAB™ (FEMLAB 2002). The method involves geometric modeling (using rational Bezier patches and curves), generation of unstructured meshes using an automatic mesh generator (created using Delaunay triangulation algorithm in MATLAB), numerical integration of the equations and boundary conditions in Gelerkin framework, and post processing using MATLAB commands. All variables are discretized with quadratic Lagrange elements.

In the laminar flow modeling, the linearized matrix resulting from the spatial discretization is solved using the Gaussian elimination method. We have a system of coupled parabolic equations in U_*, V_*, W_*, and P_* in the turbulence flow case. Due to the nonlinear nature of these equations the solution is achieved via a combination of a parametric sweeping algorithm (with the Reynolds number, Re_c, as a sweeping parameter) and Good Broyden iterative (GBIT) procedure with an exact (analytical) evaluation of the Jacobian derivatives. In this way the solution of a low Reynolds number flow is subsequently used as an initial guess for the next iteration step. This method leads to a fast and efficient convergence. To improve the efficiency of the iterative solver in relation to coping with any bad condition number, an incomplete LU factorization preconditioner is used. The convergence of the solution to the next iterative step within a given parametric sweep is assessed using the solution error criterion formulation of Deuflhard et al. (1990) given as

$$[19]\quad \frac{\sqrt{\sigma_{k+1}}}{\|\Phi_{k+1}\|} \leq \text{‘tolerance’}$$

where $\|\Phi_{k+1}\|$ is the norm of vector of unknowns at $k+1$ iterative step and the numerator is simply the norm of the preconditioned residual of the iterate $\Phi_k + 1$. A tolerance of 10^{-6} has been used in this convergence criterion. The equation for mixing length is first decomposed into Laplace and Poisson partial differential equations (PDEs) and combined with the momentum and continuity equations using a multiphysics method in FEMLAB.

Examples of used grids in both laminar and turbulent simulations are illustrated in Fig. 2 in which mesh statistics are also indicated. Because of the sharp velocity gradient expected in the viscous sublayer, more nodes are placed close to the boundaries for the turbulent case (Fig. 2*b*). This is done using selective refinement, where the triangles near the boundaries are further divided into four triangles of the same shape, but ensuring that the triangle quality (eq. [20]) is at least 0.7 for all triangles in order to decrease the number of iterations. The triangular quality has been assessed using the formula (FEMLAB 2002)

$$[20]\quad q = \frac{4\sqrt{3}a}{h_1^2 + h_2^2 + h_3^2}$$

where a is the area and h_1, h_2, and h_3 the side length of the triangle. The q term is a number between 0 and 1. If $q > 0.6$ the triangle is of acceptable quality. To ensure that the solution outputs are mesh-independent, the differences in the bulk average velocity in a sequence of successively refined meshes are compared with a preset tolerance. A tolerance of 10^{-6} has been used here.

Validation and simulations

Data for validation are scanty in this research area. Arguably the only detailed ones as of now in the literature are those of Pescod and Price (1978). These experiments were conducted in a 15 m long 300 mm diameter unplasticised poly vinyl chloride (UPVC) open-ended laboratory sewer pipe. Velocity measurements using a portable anemometer consisting of a thermister

Table 1. Comparing various models with the experiments of Pescod and Price (1978).

					Cross-sectional average velocity, U_{av}, (m/s)					
	Hydraulic parameters								Present model[a]	
Test No.	b/D	V_w (m/s)	U_w (m/s)	U_{wc} (m/s)	Experiment	USEPA	$\frac{1}{2}$-WWV	Olson and Olson et al.[b]	Turbulent	Laminar
7	0.5	0.2	0.25	0.3	0.07	0.097	0.1	0.135	0.081	0.101
8	0.6	0.8	0.96	0.65	0.2	0.342	0.4	0.356	0.272	0.36
9	0.62	0.4	0.49	0.6	0.11	0.171	0.2	0.173	0.149	0.181

[a]Gravity term included.
[b]Open-ended and smooth pipe assumption.

Fig. 2. Examples of finite element meshes; (*a*) laminar and (*b*) turbulent.

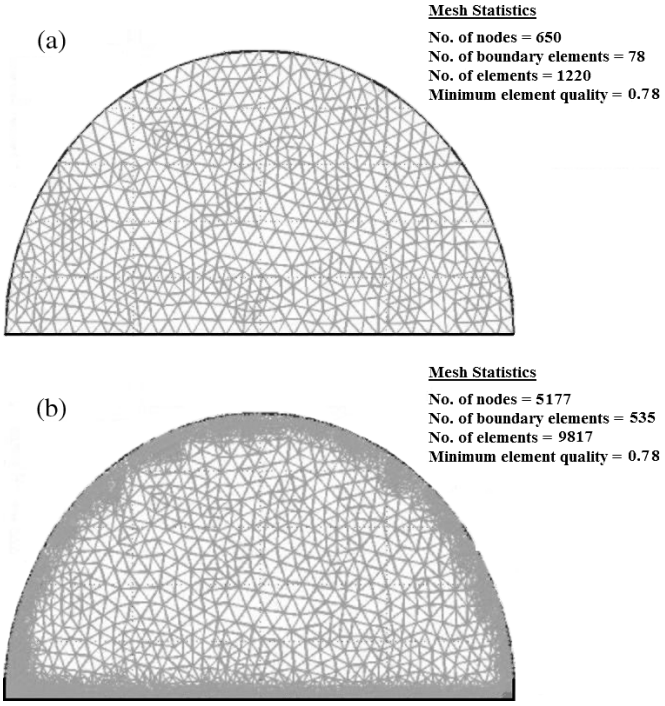

sensing device (air velocity meter, AVM) were taken at several locations over the headspace cross section in order to develop isovels for each experiment. It is unclear at what channel slopes these measurements were taken. However, based on uniform flow conditions, the channel slope can be computed using the Manning's formula $S_0 = (V_w n/R_h^{2/3})^2$, where V_w is the average water velocity, R_h is the hydraulic radius of the wetted section of the pipe, and $S_0 \approx \sin\beta$. Here n is the Manning coefficient taken as 0.009 for smooth UPVC pipe. Hydraulic parameters of the selected experiments are shown in Table 1.

The proposed models are assessed by simulating three selected experimental data (tests 7–9) from Pescod and Price (1978) that seemingly exhibit fully-developed flow characteristics and are less influenced by environmental factors in the laboratory during the time of the experiment (as pointed out in the original reference). Figures 3–5 compare simulated axial velocity contours with the selected experiments, where the isovel lines are in metres per seconds. Also displayed on the simulated velocity contours are the corresponding computed secondary flow vectors. Figure 6 also shows the comparison between experimental and computed velocity profiles for the same experiments. Data in Fig. 6 refers to the middle of the channel cross section. The analysis of the velocity profiles and isovels shows overall good accordance between the turbulent model and experimental data. The flow pattern is well predicted. Over prediction of the mean velocity profile in the top half of the headspace for tests 9 and test 7 is, however, acknowledged. Experimental data in tests 9 and 7 suggest almost zero velocity profiles for $y/b > 0.55$, which is not simulated by our model. The apparent discrepancies might be due to a number of factors. Three reasons are advanced here. The first reason could be that either our model under predicts the secondary flows or there is an additional secondary flow in the data other than that due to turbulence anisotropy. A second reason could be that there was an adverse pressure gradient counteracting the forward moving wastewater-induced flow during the time of the experiments. Under such circumstance the top part of the headspace is likely to have negative velocities that the measuring device ignored and registered as zero. A question also arises as to whether fully-developed flow conditions were attained during these experiments. For fully-developed flow to occur in noncircular ducts, the measurement section (entrance length) should be 50 times the headspace depth or longer because the secondary motion may take longer to reach a developed state (Demuren and Rodi 1984). Pescod and Price (1978) only indicated that measurements were taken slightly downstream of the center of the length that is about 7.5 m from the inlet. This does not satisfy the entrance length requirement for full flow development to occur. Also superimposed on Fig. 6 is the laminar model. It is observed that even at the channel center the laminar velocity profile is not one dimensional and that the lateral boundary influences the flow field. In all the simulations the interface is assumed to have well-organized waves of small amplitudes.

It is evident in the velocity contours (Figs. 3–5) that the primary mean velocity near the central region of the channel is advected towards the interface and the wall by the secondary currents. The pattern of air isovels, as evident in the plots, underscores the importance of the inclusion of the secondary velocities in the turbulent flow calculations. This is particularly relevant in sewer corrosion studies and emission modeling (us-

Fig. 3. Comparing contour plot of mean primary velocity for test 7, $Re_c = 3000$; (*a*) experiment and (*b*) simulated.

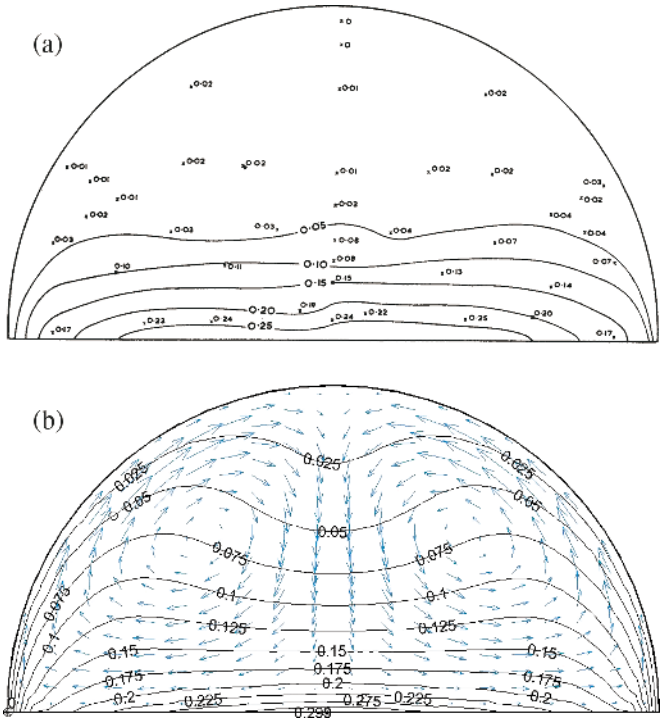

Fig. 4. Comparing contour plot of mean primary velocity for test 8, $Re_c = 7800$; (*a*) experiment and (*b*) simulated.

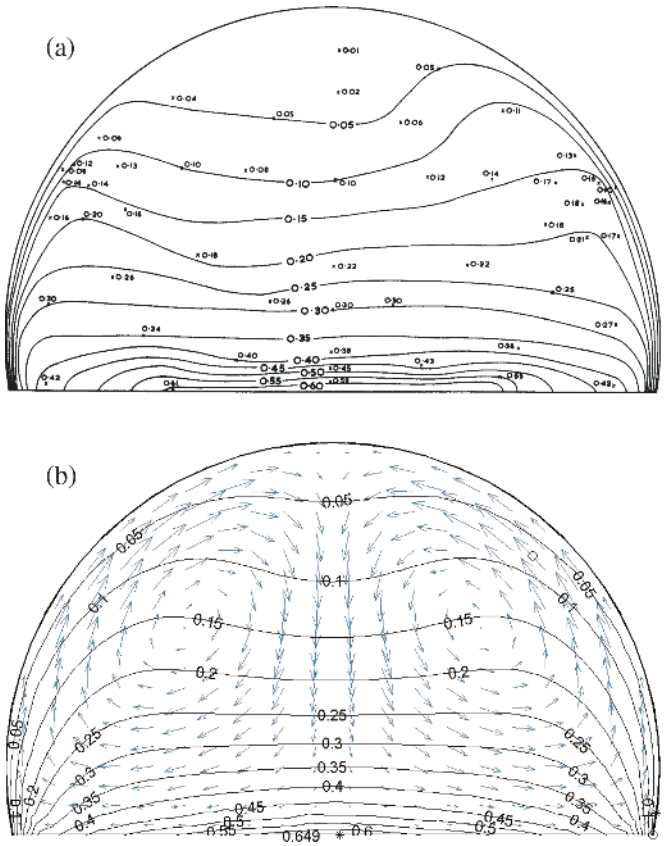

Fig. 5. Comparing contour plot of mean primary velocity for test 9, $Re_c = 7440$; (*a*) experiment and (*b*) simulated.

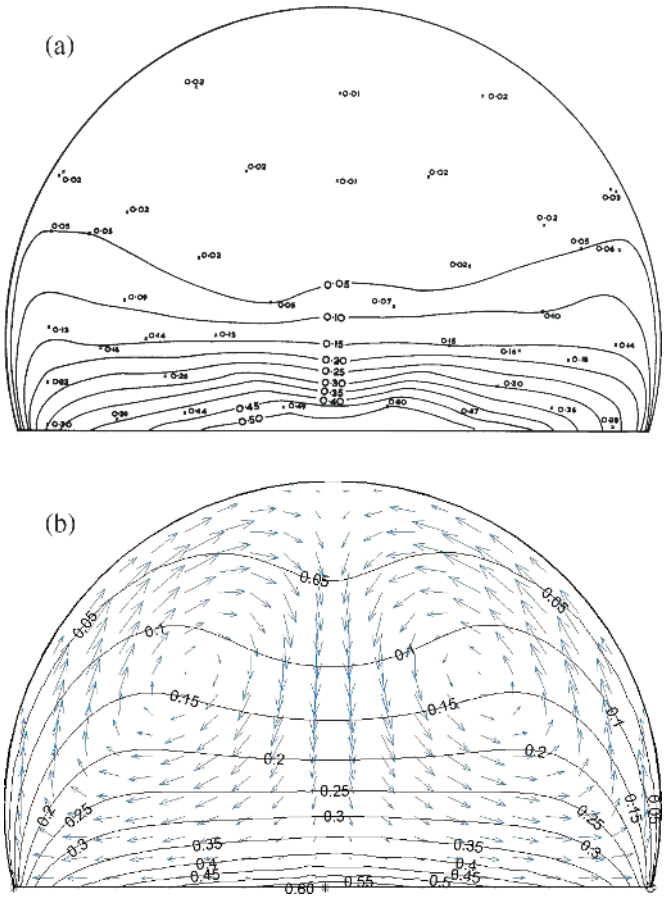

ing mass transfer techniques) where not only the mean bulk velocity is needed, but also the air flow patterns. The transfer of heat to the sewer wall and the spreading of VOCs/odours within the sewer headspace are expected to be influenced significantly by the secondary motions. In the plots (Figs. 3*b*–5*b*) a single secondary flow cell on either side of the channel quadrant is observed. The secondary flow pattern calculated here is in good agreement with that of Hoohlo (1994) who numerically simulated secondary currents in water pipe flowing partly full using an anisotropic nonlinear k–ε model for the turbulent Reynolds stresses. The pattern of the secondary flow simulated is found to be independent of Reynolds number as evident in Figs. 3*b*–5*b*. The cross-sectional average secondary velocity on the other hand is noted to depend on the relative depth b/D. This latter observation is depicted in Fig. 7 in which the cross-sectional average secondary velocity is nondimensionalized with the water surface velocity. In the figure, the secondary velocity, VW is obtained from its two components V and W, i.e., $VW = \sqrt{V^2 + W^2}$. The computed average mean secondary velocity is within 1–3% of the water surface velocity. The plot observed here shows that the strength of the average secondary velocity (dimensionalized with the water surface velocity) generally does not increase with decreasing relative depth (b/D), but stays somewhat constant in the range

Fig. 6. Longitudinal velocity profiles at headspace center; (*a*) test 7, (*b*) test 8, and (*c*) test 9.

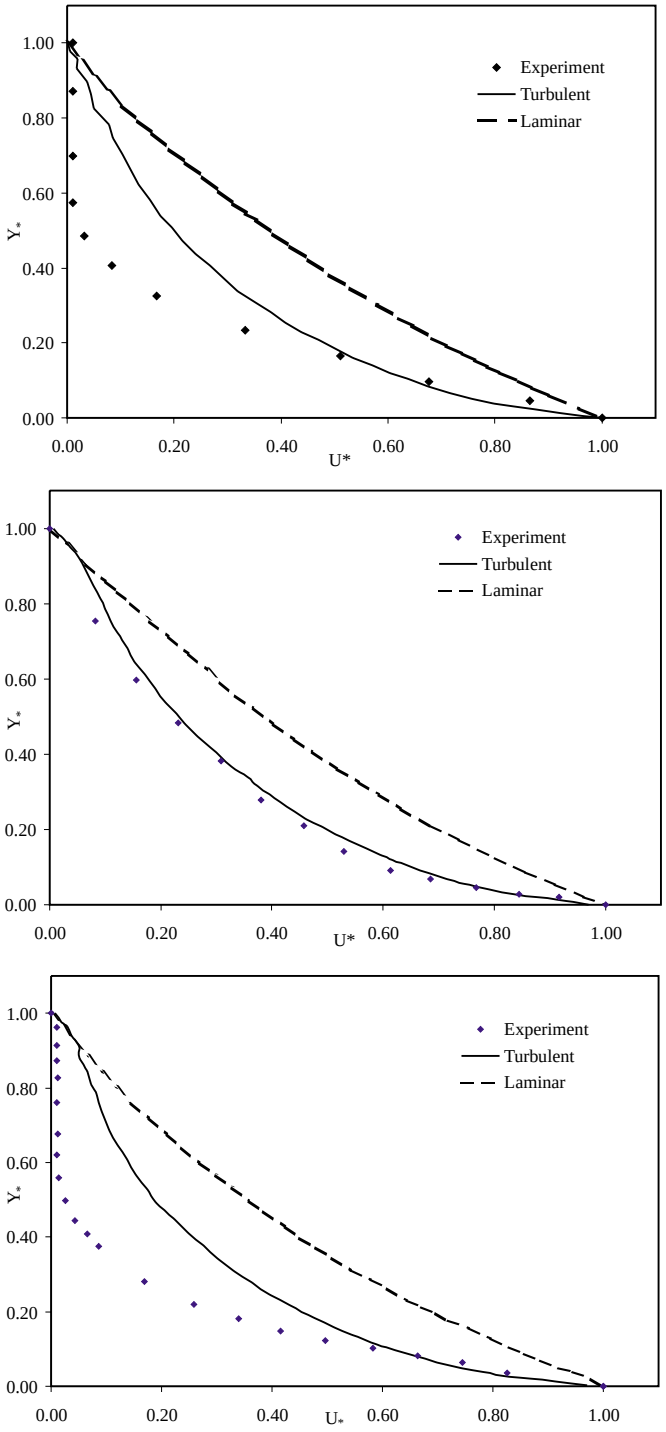

$0.30 \leq b/D \leq 0.65$. Where D is the diameter of the pipe. On one hand, the variation of the average secondary velocity nondimensionalized with the streamwise bulk velocity (VW_{av}/U_{av}) with relative depth (b/D) is found not to follow any definite pattern. The relationship is found to be spurious (not shown here), but the average secondary velocities are within 5–8% of the streamwise bulk velocity. A typical computed nondimensionalized velocity contour in laminar regime is shown in Fig. 8 for $b/D = 50\%$. Unlike the turbulent flow isovels, the laminar isovels approximately follow the shape of the sewer wall further away from the interface. In Fig. 9, calculated average velocity curves for different positions of the interface for both laminar and turbulent regimes are presented. The figure clearly shows that the streamwise bulk velocity is less than half the water surface velocity irrespective of the wastewater level or the flow regime. Given the importance of the USEPA model in the current practice of estimating ventilation rates, this model is compared with the present proposed models in Fig. 9. This model computes the average air velocity from $U_{av} = U_w C/(L + C)$, where L is the perimeter of the unwetted headspace. Calculations from our models suggest that the USEPA model is more accurate for laminar than turbulent flow. The difference in estimated average velocity between the USEPA model and the proposed laminar model is about 5%. It however overestimates the average mean turbulent velocity by about 20%. To express our simulated data in the form of the USEPA model, the following relations are obtained:

Fig. 7. Variation of simulated average mean secondary flow velocity with relative depth (b/D).

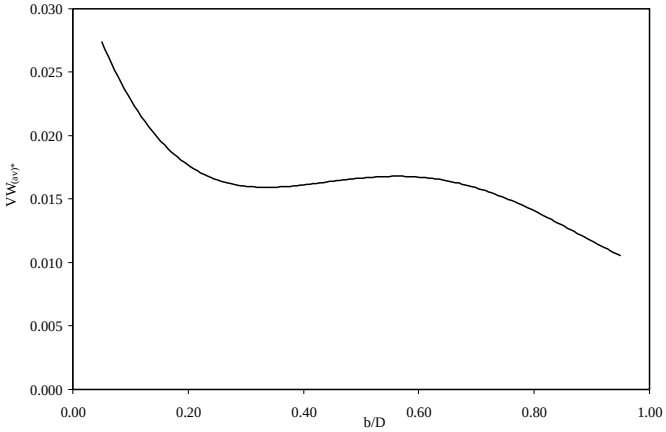

- Laminar

$$[21] \quad U_{av}/U_w = 1.028\frac{C}{(L+C)}, \quad R^2 = 0.993$$

- Turbulent

$$[22] \quad U_{av}/U_{wc} = 0.8560\frac{C}{(L+C)}, \quad R^2 = 0.994$$

where R is the coefficient of determination. These equations are plotted together with the simulated data in Fig. 10. Also shown in the same figure is the USEPA model. Thirty simulated points have been used in fitting the above relations. It can be deduced from eqs. [21] and [22] that the ratio of the nondimensionalized laminar average streamwise velocity to the corresponding turbulent case is about 1.2.

Finally, comparisons of average mean velocity with the present models, the $\frac{1}{2}$-wastewater velocity model (hereafter referred

Fig. 8. Typical nondimensionalized velocity (U/U_w) contour distribution for $b/D = 50\%$ in laminar flow regime.

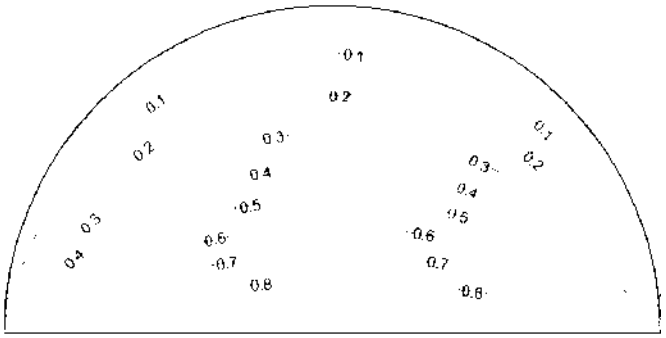

Fig. 9. Average longitudinal velocity curves as a function of the relative depth (b/D); Also compared is the USEPA (1994) model.

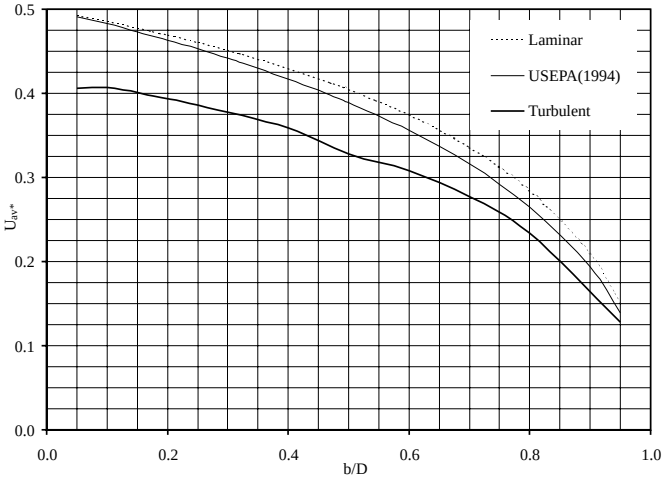

Fig. 10. Average longitudinal velocity plot as a function of headspace perimetric shape factor.

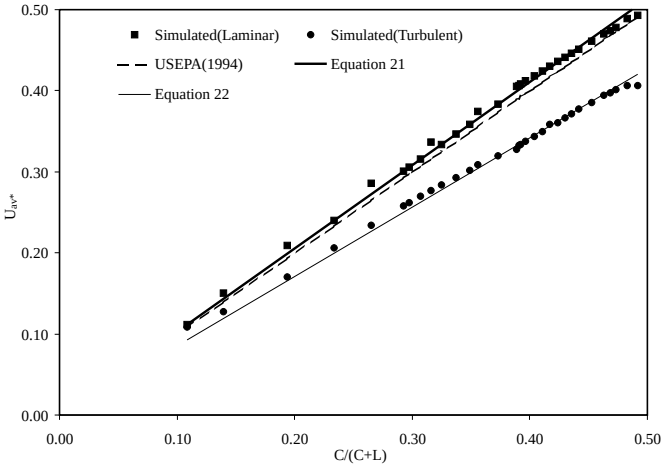

to as $\frac{1}{2}$-WWV model), Olson and Olson et al.'s model, and the USEPA model are made with the experiments of Pescod and Price as shown in Table 1. As can be seen in the table, all the models over predict the measured average air velocity. High predictions from Olson and Olson et al.'s model are possibly due to the interfacial drag coefficient expression used in their model. It must be mentioned here that the physical processes at the interface of a horizontal stratified air–water flow (where each fluid flows under its own driving force in addition to the interfacial shear) are quite different from those in air-wastewater flow in sewers where the only force driving the air in this case is that of the wastewater drag. Their model, which is in a form of a nonlinear algebraic expression, has been solved using a nonlinear minimization algorithm in MATLAB.

Overall, it is demonstrated that the present models are quite useful and cost effective in obtaining detailed flow field information. Particularly, it is valuable in understanding the flow feature changes due to changes in wastewater level and flow rate.

Conclusions

Models that can be used to assess the magnitude and nature of sewage drag effect in transporting air along sewer conduits have been presented. The effect of interfacial drag of wastewater is conceptually viewed as a Couette flow. The outputs from these models are essential for the implementation of any efficient odour and corrosion control technology in both turbulent and laminar flow regimes. In the turbulent modeling, the Reynolds equations are closed with a relatively simple turbulence model that consists of an eddy viscosity hypothesis for the shear stresses and a semi-empirical model for the normal stresses. Finite element solution of the parabolic approximation of the model equations gives good secondary flow patterns as well as longitudinal velocity distribution in the headspace cross section. The models have been validated with experimental data from Pescod and Price (1978). Overall, it is found that the models are capable of reproducing observed flow characteristics, and the agreement with experimental data is also favorable. Using the models we have presented average velocity curves and formulae that can be used for calculating the longitudinal average velocity relative to the wastewater. These curves and formulae suggest that the amount of ventilation induced by wastewater drag is dependent upon the wastewater surface velocity, the unwetted wall perimeter, interfacial surface width, and the headspace depth.

Specifically, the following conclusions can be drawn:

(1) The previously available ventilating models used for emission estimates and in corrosion modeling are incapable of detailing the air flow structure and generally over predict the mean velocity, especially in turbulent flow.

(2) To understand the flow structure in the headspace under different flow conditions, it is necessary to elucidate the secondary current structures in turbulent flow regimes. Although these secondary velocities are within 5–8% of the streamwise bulk velocity, these currents may have important consequences on the air flow field.

(3) An interesting relationship is found to exist between the cross-sectional average secondary velocity (nondimensionalized with the water surface velocity) and the relative

depth (b/D). The relationship indicates that although the strength of the cross-sectional average secondary velocity depends on the relative depth, it remains almost constant for headspace proportional depth range of about 30–65%. The average secondary velocity is calculated to be within 1–3% of the water surface velocity.

(4) The isovels in the laminar flow regime decrease from the air–water interface with increasing vertical distance from the water surface and follow approximately the wall boundary.

(5) The computed streamwise bulk velocity is consistently less than half the water surface velocity. This is found to be independent of the wastewater level or the flow regimes studied.

In spite of the progress and the optimistic results reported herein, there are still significant areas where modeling refinements are needed. For instance the effects of fully rough interfacial waves and roughness of the collection conduit wall, subjects not addressed in this paper, still remain major challenges.

Acknowledgements

We gratefully acknowledge financial support from the Natural Sciences and Engineering Research Council of Canada (NSERC) through a research grant to the second author and the University of Alberta Research Assistantship to the first author. The authors are also grateful to Professor Warren M.B. Pescod of Motherwell Bridge, England, for providing us with his experimental data.

References

Bowker, R.P.G., Smith, J.M., and Webster, N.A. 1989. Odor and corrosion control in sanitary sewerage systems and treatment plants. Hemisphere Publishing Corporation, New York.

Czernuszenko, W., and Rylov, A. 2002. Modeling of three-dimensional velocity field in open channel flows. J. Hydraul. Res. **40**(2): 135–143.

Demuren, A.O., and Rodi, W. 1984. Calculation of turbulence-driven secondary motions in non-circular ducts. J. Fluid Mech. **140**: 189–222.

Deuflhard, P., Freund, R., and Walter, A. 1990. Fast secant methods for the iterative solution of large nonsymmetric linear systems. IMPACT Comp. Sci. Eng. **2**: 244–276

Edwini-Bonsu, S., and Steffler, P.M. 2003. Dynamics of air flow in sanitary sewer conduits due to differential pressure. J. Environ. Eng. ASCE. Submitted.

FEMLAB. 2002. Version 2.3a. Comsol Inc.

Gerard, R. 1978. Secondary flow in non-circular conduits. J. Hydraul. Div. Am. Soc. Civ. Eng. **104**(HY5): 603–616.

Hoohlo, C.A. 1994. A numerical and experimental study of open channel flow in a pipe of circular cross-section with a flat bed. Ph.D. thesis. University of Newcastle, upon Tyne, UK.

Lam, C.K.G., and Bremhorst, K. 1981. A modified form of the k–ε model for predicting wall turbulence. J. Fluids Eng. **103**: 456–460.

Matos, J.S., and de Sousa, E.R. 1992. The forecasting of hydrogen sulphide gas build-up in sewerage collection systems. Water Sci. Technol. **26**(3–4): 915–922.

Nordsveen, M., and Bertelsen, F.A. 1996. Waves and secondary flows in stratified gas/liquid duct flow. *In* Waves and non-linear processes in hydrodynamics. *Edited by* J. Grue, B. Gjevik, and J.E. Weber. Kluwer Academic Publishers, Dordrecht , The Netherlands, pp. 279–290.

Odor and Corrosion Technology Consultants, Inc. 1999*a*. The use of modeling techniques to evaluate and correct odor releases from trunk sewers. TM No.4, City of Edmonton Odour Control Project, Edmonton, Alta.

Odor and Corrosion Technology Consultants, Inc. 1999*b*. Trunk sewer odor monitoring program. TM No.1, City of Edmonton Odour Control Project, Edmonton, Alta.

Olson, D. 1996. Gas exchange rates between industrial process drains and the ambient atmosphere. M.Sc. thesis. University of Texas, Austin, Tex.

Olson, D., Rajagopalan, S., and Corsi, R.L. 1997. Ventilation of industrial process drains: mechanisms and effects on VOC emissions. J. Environ. Eng. **123**(9): 939–947.

Pescod, M.B., and Price, A.C. 1978. A study of sewer ventilation for the Tyneside sewerage scheme. Final research report, Department of Civil Engineering, University of Newcastle upon Tyne, UK.

Pescod, M.B., and Price, A.C. 1981. Fundamentals of sewer ventilation as applied to the Tyneside sewerage scheme. Water Pollut. Control, **90**(1): 17–33.

Pescod, M.B., and Price, A.C. 1982. Major factors in sewer ventilation. J. Water Pollut. Control Fed. **54**(4): 385–397.

Pomeroy, R. 1945. Pros and cons of sewer ventilation. Sewage Works J. **17**(2): 203–208.

Quigley, C.J., and Corsi, R.L. 1995. Emission of VOCs from a municipal sewer. J. Air Waste Manage. Assoc. **45**(5): 395–403.

Robert, J-L., Khelifi, M., and Ghanmi, A. 1998. Use of the mixing length concept to correctly reproduce velocity profiles of turbulent flows. Can. J. Civ. Eng. **25**:232–240.

Rodi, W. 1984. Turbulence models and their application in hydraulics. A state of the art review. International Association for Hydraulic Research, Delft, The Netherlands.

Sinai, Y.L. 1983. A Charnock-based estimate of interfacial resistance and roughness for internal, fully-developed, stratified, two-phase horizontal flow. Int. J. Multiphase Flow, **9**(1): 13–19.

Thistlethwayte, D.K.B. 1972. The control of sulphides in sewer systems. Ann Arbor Science Publishers, Ann Arbor, Mich. pp. 47–64 and pp.142–168.

Tominaga, A., Nezu, I., Ezaki, K., and Nakagawa, H. 1989. Three-dimensional turbulent structures in straight open channel flows. J. Hydraul. Res. **27**(1): 149–173.

US Environmental Protection Agency (USEPA). 1994. Air emission models for waste and wastewater. EPA-453/R-94–080A-Part 1.

Vlachos, N.A, Paras, S.V., and Karabelas, A.J. 1999. Prediction of holdup, axial pressure gradient and wall shear stress in wavy stratified and stratified/atomization gas/liquid flow. Int. J. Multiphase Flow, **25**: 365–376.

Wilcox, D.C. 2000. Turbulence modeling for CFD. 2nd ed. DCW Industries, Inc., La Cañada, Calif.

List of symbols

A_{wy}, A_{vy}, A_{wn}, A_{vn}	empirical constants for turbulent intensity distributions
b	maximum headspace depth
B_{wy}, B_{vy} B_{wn}, B_{vn}	empirical constants for turbulent intensity distributions
C	width of the air–water interface
D	sewer pipe diameter
g	acceleration due to gravity
h	channel flow depth
k	turbulent kinetic energy
k_s	effective roughness height
k_s^+	dimensionless effective roughness height ($k^+ = u_{\tau i} k_s / v$)
l_m	mixing length
L	perimeter of the unwetted headspace
n	normal to or from the boundary or Manning coefficient
P	mean pressure
R	coefficient of determination
R_h	hydraulic radius of water section
Re	Reynolds number (Re $= U_w b/v$ and $\mathrm{Re}_c = U_{wc} b/v$)
S_0	channel slope
t	time
u_τ	shear velocity
U	longitudinal mean velocity
U_{av}	bulk average velocity
U_w	average water surface velocity
U_{wc}	water surface velocity at channel center
U_{ws}	interfacial velocity
u', v', w'	velocity fluctuations in x, y, and z directions, respectively
$\sqrt{\overline{v'^2}}$, $\sqrt{\overline{w'^2}}$	root-mean-square of turbulence in y and z directions, respectively
V, W	secondary velocities in y and z directions, respectively
VW	magnitude of the secondary flow vectors (V, W)
V_w	average water velocity
x	axial–longitudinal Cartesian co-ordinate
X_*	$= x/b$
y	vertical Cartesian coordinate
Y_*	$= y/b$
y^+	normalized wall distance ($y^+ = u_{\tau i} n_i / v$)
z	transverse and (or) lateral Cartesian coordinate
Z_*	$= z/b$
β	sewer pipe slope
κ	von Karman's constant = 0.41
v	kinematic viscosity (= 1.5×10^{-5} m^2/s); turbulent eddy viscosity (v_t)
ρ	mass density of air (= 1.28 kg m^{-3})
ε	rate of turbulent kinetic energy dissipation

Subscripts

av	spatial average
i	pertaining to the interface
i, j, k	coordinates directions; Tensor indices
t	turbulent
w	pertaining to the wall or water
*	dimensionless